

Effect of ultralight dark matter on compact binary mergers

Kabir Chakravarti,^{1,*} Soham Acharya,^{2,†} Sumanta Chakraborty,^{3,‡} and Sudipta Sarkar^{2,§}

¹*CEICO, Institute of Physics of the Czech Academy of Sciences, Na Slovance 1999/2, 182 00, Prague 8, Czech Republic*

²*Indian Institute of Technology, Gandhinagar, Gujarat 382055, India*

³*School of Physical Sciences, Indian Association for the Cultivation of Science, Kolkata 700032, India*

(Dated: March 26, 2025)

The growing catalogue of gravitational wave events enables a statistical analysis of compact binary mergers, typically quantified by the merger rate density. This quantity can be influenced by ambient factors, following which, in this work we have investigated the impact of dark matter environment on the merger statistics. We construct a baseline astrophysical model of compact binary mergers and extend it by incorporating a model of ultra light dark matter, which affects the orbital evolution of binaries through accretion and dynamical friction. Our analysis of the merged population of binary progenitors demonstrates that, compared to the baseline model, ULDM can significantly alter the merger statistics when its ambient density becomes larger than $10^4 \text{GeV}/\text{cm}^3$. A comparison with the gravitational wave data from the GWTC-3 catalogue provides insight into potential observational signatures of the ULDM in merger events, leading to possible constraints on the existence and density of dark matter distribution in galaxies.

I. INTRODUCTION

Understanding the nature of the compact objects, e.g., black holes (BHs) [1, 2], neutron stars (NSs) [3, 4] and exotic compact objects (ECOs) [5], that exist in our universe and assessing their environments has been one of the key research areas of gravitational physics. This will not only provide information about the properties of these compact objects and strong gravity regime that these objects live in, but also about their environments [5, 6]. The upshot being, we will be able to confidently comment, whether general relativity is the theory of gravity describing our universe even in the strong field regime, as well as prove the existence of objects, that are more compact than NSs, but less compact than BHs [7–10]. These will revolutionize the current understanding of our universe in many possible ways .

However, the significance of studying compact object environments extends beyond these aspects. It can also reveal crucial information about a variety of astrophysical phenomena, including the presence of a third body—such as exoplanets or stars—orbiting these compact objects [11, 12]. Additionally, such investigations can shed light on the existence and distribution of dark matter (DM) [13–15]. In this work, we focus specifically on exploring the presence and properties of DM based on current observational data.

As far as assessing the physics on and around compact

objects¹ are considered, the black hole shadow [16] and the gravitational wave (GW) observations are most effective. While, observations involving black hole shadow are severely limited, in the sense that only two BHs, the M87* and the Sgr A* has been pictured so far [17, 18], numerous GWs from compact binary coalescence have already been detected through the LIGO-VIRGO-KAGRA (LVK) collaboration [4, 19] and the detection rate is expected to grow exponentially with future generations of GW detectors [20, 21]. Thus, we will focus on understanding the properties of DM distribution around compact objects through the GW observations.

The fact that our universe entails more invisible matter than visible ones had its origin in the observations involving rotation curves of galaxies, where it was observed that the almost-constant rotation curves can be beautifully explained by postulating the existence of such invisible or, dark matter [22]. Besides, several other clinching astrophysical evidences, e.g., bullet cluster, dwarf spheroidal galaxies, gravitational lensing have been put forward in support of the DM hypothesis [23–25]. Similarly, in the context of cosmology as well, the matter content of our universe requires the existence of DM, whose abundance is at least five times larger than those in the standard model of particle physics [26]. In particular, according to the current paradigm of cosmology, DM plays a crucial role in the formation of structures in our universe, as they are the first one to collapse into structures called DM halos, into which visible matter falls, leading to individual galaxies. Observational constraints from structure formation [27], Lyman- α measurements [28] and lensing [29] restrict the composition of DM at

* chakravarti@fzu.cz

† acharyasoham@iitgn.ac.in

‡ tpsc@iacs.res.in

§ sudiptas@iitgn.ac.in

¹ Throughout this work, by compact objects, we will mean objects, whose compactness is larger or equivalent to that of a typical NS.

length scales $\gtrsim 100$ Mpc to be cold (CDM). In other words, DM behaves as a pressure-less fluid at these scales. This gives rise to the well-known Λ CDM paradigm, the standard model of cosmology. However, at small scales, the CDM hypothesis faces serious challenges, the ‘Core-Cusp problem’ [30], the ‘Galactic Morphology problem’ [31], and the ‘Missing satellites problem’ [32] are to name a few of them. Side by side, the observational constraints on the nature of DM are also much weaker at galactic length scales of $\sim 10 - 100$ Kpc.

One way to circumvent this difficulty, is to assume that DM is no longer cold in these regions, rather they form a condensate. This is where, the Ultra-Light DM (ULDM) plays a pivotal role [33] and can alleviate some of the challenges faced by the CDM scenario. In this formulation, DM is thought to be composed of light bosons, which forms a condensate at galactic length scales, thereby deviating from the CDM hypothesis, while smoothly joins with CDM at larger length scales, without violating any observational constraints [33]. Moreover, such light bosons have also been shown to arise from simple extensions of the standard model for particle physics, e.g., models involving axions [34]. All of these make ULDM models a viable alternative to the CDM at the galactic scale.

At the same time, as elaborated above, mergers of compact objects have now become a regular occurrence since their discovery in 2015 by the LVK detectors, which have now detected $\mathcal{O}(100)$ merger events. This presents an interesting possibility to check the existence of ULDM at galactic scales through GW observations. The basics are as follows, in the presence of an environment consisting of ULDM, the binary objects are moving around each other not in vacuum, but in a medium composed of ULDM. Consequently, both the objects in the binary will experience a viscous drag due to the presence of ULDM medium, which can also accrete into the individual objects. The calculation of the viscous drag force in the relativistic context was shown in [35] to be a straight generalisation of the Newtonian dynamical friction formula derived by Chandrasekhar [36]. It turns out that both the dynamical friction, as well as accretion, as described above, alters the binary inspiral dynamics and leave their signature on the binary phasing. This concept was used [37] to constrain the ambient density of baryons from specific merger events in GWTC2 [38]. More recently another work [39] had also used ULDM interactions to distinguish different surface properties of the compact objects, though using extreme-mass-ratio inspirals.

In this work, we start with a simple implication of the previous literature, namely that an environment is likely to alter the merger timescales for a binary system. Given this alteration, we investigate if the ULDM environment can leave its biasing upon the statistics of compact binary mergers. In other words, we want to understand how big or small the effect of ULDM dynamical friction and/or accretion is upon the

number of mergers happening per unit redshift per unit observer time per unit co-moving volume, the so-called ‘astrophysical merger rate density’. Due to the inherent astrophysical uncertainty in the star formation rate, and its modelling, the results presented here will not be conclusive, rather will provide a proof-of-principle that DMs and their properties can be understood using merger rate density. Further astrophysical refinements will make our conclusions more robust, which we will come back to in a subsequent publication. Our paper is organised as follows: in Section II, we review some of the key previous results which are necessary for our subsequent calculations involving the biasing effects expected for mergers in an ULDM environment in Section III. We take help of toy problems to demonstrate the calculations for individual binaries in Section III A and populations Section III B. We present our results for the astrophysical merger rate of compact objects in presence of an ULDM environment in Section IV. We finally present our conclusions in Section V.

Conventions — Throughout this paper we will use geometric units, namely $G = c = 1$. Note that we *do not* use $\hbar = 1$. Also, we work in four spacetime dimensions, with mostly positive signature convention, such that the flat metric becomes $\eta_{\mu\nu} = \text{diag.}(-1, +1, +1, +1)$.

II. BINARY MERGERS IN AN ULTRA-LIGHT DARK MATTER ENVIRONMENT

In this section, we will present a brief review of the framework and the implications of the ULDM environment on the merger rate of binary compact objects. We start by reviewing the computation of accretion and dynamical friction experienced by a compact object in this environment, following [35, 39]. Our implementation of these effects into the dynamics of binary mergers and their rate will follow from analogous works involving visible matter environments [37, 40].

A. Framework

We consider the ULDM to be represented by a light scalar field, which satisfies the massive Klein-Gordon equation

$$\square\Phi - \mu^2\Phi = 0, \quad (1)$$

where $m_\Phi = \hbar\mu$ is the mass of the scalar field. The box operator in Eq. (1) is taken to be a non-trivial background given by the geometry of the massive compact object. If the compact object is non-rotating, the geometry will be that of Schwarzschild, while for rotating compact object the geometry will be given by Kerr metric. Then, following [39], we look for solutions for the scalar field at the rest frame of the compact object, which at large distance from

the compact object, behave as plane waves,

$$\Phi(t, r) \sim \sqrt{\frac{\rho_0}{\mu}} e^{i(\omega t - k_\infty r)}. \quad (2)$$

Here, ρ_0 is the homogenous rest mass density of the scalar field, and $k_\infty = \sqrt{\omega^2 - \mu^2}$. In general, the density ρ_0 of the ULDM, appearing above, will be dependent on the distance from the galactic halo, however, we will assume it to be homogeneous, since our interest is to observe if there is at all any effect of DM on the binary merger rate. Subsequently, one can refine the analysis further, by introducing more realistic density profiles for ULDM. Note that for $\omega > \mu$, the scalar particle scatters off the compact object, while for $\omega < \mu$, the scalar particles form quasi-bound states. In this computation, we will assume that $\omega > \mu$, along with $M\omega \ll 1$, which is the prime reason for studying the ultra-light sector, so that the above conditions are trivially satisfied. The relative velocity of the BH with respect to the DM particles is given by $v^i = -k_\infty^i/\omega$, with $|k_\infty^i| = k_\infty$. Therefore, it follows that, $\omega = \gamma\mu$ and $k_\infty^i = -\gamma\mu v^i$, with $\gamma = 1/\sqrt{1 - v^2}$ is the Lorentz factor.

The computation of the rate of accretion and dynamical friction follows the below steps — (a) one solves for the radial part of Eq. (1) in the Kerr background, in the asymptotic and the near-horizon regime; (b) for the near-horizon solution, one imposes reflecting boundary conditions, when these binary objects are stars, and impose purely ingoing boundary conditions for BHs; (c) the asymptotic limit of the near-horizon solution is matched with the near-zone limit of the asymptotic solution; (d) this matching provides ratio of reflected and incident amplitudes of the scalar field, which in turn provides the accretion rate and force due to dynamical friction. In the frame of the object moving through DM distribution, these read [35, 39],

$$\dot{M} = \int_\infty r^2 T_{tr} d\Omega_2 = \rho A_h \left(\frac{e^{\pi\eta}\pi\eta}{\sinh(\pi\eta)} \right) \left(\frac{1-R}{1+R} \right), \quad (3)$$

$$F^i = \int_\infty r^2 T_r^i d\Omega_2 = -\frac{4\pi\rho M^2}{v^2} (1+v^2)^2 \mathcal{D}\zeta^i - \dot{M}v^i. \quad (4)$$

The quantity R , appearing above, in the expression for \dot{M} , is unity for stars, and vanishes for BHs. Thus the above expression for accretion is relevant for BHs alone. Here, $T_{\mu\nu}$ is the energy-momentum tensor of the scalar field, ζ^i is the direction from which the scalar waves impinges on the BH at rest, $\eta = -\{\gamma\mu M(1+v^2)/v\}$, $\rho = \gamma^2\rho_0$ and $\mathcal{D} = \ln\Lambda - \text{Re}[\Psi(1-i\eta)]$. The quantity $\Psi(x)$ is the di-gamma function and $\Lambda = \gamma v \mu b_{\text{max}}$, with b_{max} being the maximum impact parameter. Note that $\gamma v \mu$ is the inverse of the de-Broglie wavelength associated with the DM particles. Finally, the quantity $A_h = 4\pi(r_+^2 + a^2)$ is the horizon area, with $r_+ = M + \sqrt{M^2 - a^2}$, being the location of the event horizon, and $J = aM$ is the angular momentum of the BH. In the expression for force experienced by the compact object due to scattering from

ULDM, the first term represents the gravitational drag from the surrounding ULDM field, and the second term accounts for momentum loss due to accretion.

Since we observe the GWs emitted from such systems at infinity, our frame of reference coincides with the rest frame of the scalar field. Hence all the expressions ought to be written in the rest frame of the scalar field. In this frame, the objects move in their binary orbits through a homogenous ULDM density. This is simply achieved by the following transformations: $\dot{M}' = (\dot{M}/\gamma)$ and $F'_i = F_i + \dot{M}v_i$. Then, it turns out (see [39] for the detailed calculation) that the accretion rate of an object of mass M and angular momentum J moving through the ULDM medium with an orbital speed v , in the rest frame of the DM, is given by,

$$\dot{M}' = \hbar n \omega A_+ \left(\frac{e^{-\pi\eta}\pi\eta}{\sinh(\pi\eta)} \right) \left(\frac{1-R}{1+R} \right), \quad (5)$$

where, $n = (\rho/m_\Phi)$ is the number density of the ULDM particles, and we assume complete absorption if the object is a BH ($R = 0$) and complete transmission in all other cases ($R = 1$). Similarly, the dynamical friction force acting on the object in the rest frame of the DM is given by

$$\vec{F}' = -\frac{4\pi\rho M^2}{v^2} (1+v^2)^2 \mathcal{D}\vec{\zeta} = -\frac{4\pi\hbar n \eta^2}{\mu} \Delta\Psi\vec{\zeta}, \quad (6)$$

where, $\mathcal{D} = \Delta\Psi = \text{Re}[\Psi(1+\ell_m+i\eta) - \Psi(1+i\eta)]$ with Ψ being the digamma function and ℓ_m the cut-off in the angular harmonic corresponding to the maximum impact parameter of the object b_{max} . As evident, the dynamical friction is independent of the details of the nature of the compact object, while accretion is dependent on the compact object. We will show the effect of accretion on binary merger rate in Section II B. Multiplying the dynamical friction force by the relative speed v between the compact objects, we can finally deduce the power dissipation through the dynamical friction as

$$P_{\text{df}} = \vec{F}' \cdot \vec{v} = -\frac{4\pi\hbar}{\mu} n v \eta^2 \Delta\Psi. \quad (7)$$

This dissipative term will add up to the quadrupolar radiation emitted from the binary inspiral, leading to faster energy loss from the system. This results into faster inspiral, and hence reduces the merger time, having impact on the rate of binary merger. We will implement this for binary orbits in the subsequent section.

B. Implementation in binary inspiral

Following the outlines of Section II A, we note that the motion of binary objects through the DM environment creates an extra dissipation force, which in the scalar's rest field gives rise to an additional loss of power, given by P_{df} . In the case of a binary orbit, the consequence

being, the loss of the total orbital energy of the binary. In addition to this dissipation due to DM, there is also a dissipation from the emission of GWs, which at leading order is given by [41],

$$P_{\text{gw}} = \frac{32}{5} \frac{m_{\text{r}}^2 M_{\text{T}}^3}{a^5}, \quad (8)$$

where, $m_{\text{r}} = M_1 M_2 / (M_1 + M_2)$ and $M_{\text{T}} = M_1 + M_2$ are the reduced mass and the total mass of the particular binary, respectively, with individual masses being M_1 and M_2 . The quantity a is the binary separation and is related to the orbital velocity v , as well as the orbital frequency Ω of the reduced mass system by $v^2 = (M_{\text{T}}/a) = (M_{\text{T}}\Omega)^{2/3}$. Note that the frequency of the emitted GW is twice of the orbital frequency. Following the implementation of [40], the equation for orbital phasing of GW becomes

$$\begin{aligned} \frac{d\phi}{dt} &= \Omega, \\ \frac{dE_{\text{orb}}}{dt} &= -P_{\text{gw}} - P_{\text{df}}, \end{aligned} \quad (9)$$

where, the orbital energy E_{orb} is given at the leading order by $E_{\text{orb}} = -(1/2)m_{\text{r}}v^2$. We can then substitute for E_{orb} along with the expressions of P_{df} and P_{gw} from Eq. (7) and Eq. (8) to obtain,

$$-\frac{1}{2} \frac{d}{dt} \left(\frac{m_{\text{r}} M_{\text{T}}}{a} \right) = -\frac{32}{5} \frac{m_{\text{r}}^2 M_{\text{T}}^3}{a^5} - \frac{4\pi\hbar n}{\mu} \sum_{i=1}^2 \eta_i^2 v_i \Delta\Psi_i, \quad (10)$$

where the sum over i represents a summation over the components of the binary. Then it is easy to see from the motion of the reduced mass that $v_i = (m_i/M_{\text{T}})v = (m_i/M_{\text{T}})\sqrt{M_{\text{T}}/a}$, where i, j are just distinct labels for the binary components and not spatial indices. We should also note that the time differentiation operator on the left hand of Eq. (10) will also hit both m_{r} and M_{T} , where the corresponding expressions have to be substituted from Eq. (5). In this way we see that we end up with a differential equation in terms of the binary's orbital separation a . The numerical evolution of Eq. (10) determines the dynamics of the binary in question, which will be different from the vacuum evolution, due to the presence of dynamical friction.

III. DARK MATTER ENVIRONMENT AND MERGER STATISTICS

Here, we will present our results regarding merger statistics of binary evolution in the environment of ULDM and shall quantify the effects of ULDM on compact binary mergers. We start by discussing the effects of environment on individual binaries and then focus on the effect on binary population and their merger rate.

A. Individual Binaries

We show the effect of the presence of ULDM on the merger timescale of individual binaries in this section. For that we start with a chosen mass configuration of binary main sequence stars as progenitors and track their merger status by evolving Eq. (9) to obtain the binary separation a with time. To do this consistently, we require a proper transformation function when a progenitor star reaches its stellar endpoint. We implement this by a simple mass-transfer function [42] to determine the mass of the evolutionary remnant of the main sequence star. In reality, such endpoints of massive main-sequence stars are usually accompanied by novae, which are highly model dependent and is likely to add a further layer of uncertainty to our baseline model, but will not significantly contribute to an understanding of the effects of ULDM on binary merger. Nevertheless, we need to implement a model to facilitate mergers and not disrupt them. To do this, we adopt a method similar to the evolution method previously implemented in [43] with the notable exception that our method does not model for any additional kick at the endpoint of main-sequence evolution. Thus we will potentially be biased towards higher merger rate. To determine the shift in the orbital separation a due to the stellar endpoint, we consider the variation in the angular momentum $L := m_{\text{r}} a^2 \Omega$ and use the Kepler's third law $\Omega^2 a^3 = M_{\text{T}}$, to obtain,

$$\left(\frac{\delta a}{a} \right) = 2 \left(\frac{\delta L}{L} \right) - 2 \left(\frac{\delta m_{\text{r}}}{m_{\text{r}}} \right) - \left(\frac{\delta M_{\text{T}}}{M_{\text{T}}} \right), \quad (11)$$

$$\left(\frac{\delta \Omega}{\Omega} \right) = -3 \left(\frac{\delta L}{L} \right) + 3 \left(\frac{\delta m_{\text{r}}}{m_{\text{r}}} \right) + 2 \left(\frac{\delta M_{\text{T}}}{M_{\text{T}}} \right), \quad (12)$$

where δx represents the change in a quantity x before and after the stellar endpoint. We can then eliminate $(\delta L/L)$ from Eq. (11) to obtain $3(\delta a/a) = (\delta M_{\text{T}}/M_{\text{T}}) - 2(\delta \Omega/\Omega)$. From the mass-transfer function implementation of [42] the final mass is less than the initial mass because a nova usually involves ejection of mass. Therefore, it follows that $(\delta M_{\text{T}}, \delta m_{\text{r}}) < 0$. We further assume that $(\delta \Omega/\Omega) \geq 0$, which ensures that the binary separation does not *increase* across the stellar endpoint. Further, from the above expressions it follows that $|\delta a/a| \geq (1/3)|\delta M_{\text{T}}/M_{\text{T}}|$. From this, we finally make our choice of δa across stellar endpoint as

$$\delta a = \left(\frac{\delta M_{\text{T}}}{M_{\text{T}}} \right) a. \quad (13)$$

Note that, the above relation ensures that $\delta M_{\text{T}} < 0$, implies $\delta a < 0$, since both a and M_{T} are positive definite quantities. This completes the formulation of our baseline model, which is constructed in the absence of any ULDM environment.

Before moving further we note that the overall effect of the ULDM environment is through accretion and dynamical friction. As already emphasized, Eq. (6) depicts that

the drag term acts universally upon any object, but the accretion term is dependent upon the nature of the surface reflectivity, which will vanish for a BH, while will be unity for a star. Thus the evolution of the binary separation will be different for stars and BHs. With this specific model, we consider the following example involving a binary progenitor configuration of total mass and mass-ratio being $M_{\text{T}}^{\text{P}} = 45M_{\odot}$ and, $q^{\text{P}} = 0.8$, respectively, for two different starting redshift and for two cases with and without ULDM environment. Quantities related to the progenitor stars will be denoted with a superscript P. At this point we remark that further simplicity is maintained in our baseline model by not considering properties like orbital eccentricity and/or BH spins. Under these simplifying assumptions, any difference in the final binary configuration between the baseline model and the model with ULDM can be thought of as being solely due to the presence of the ULDM environment.

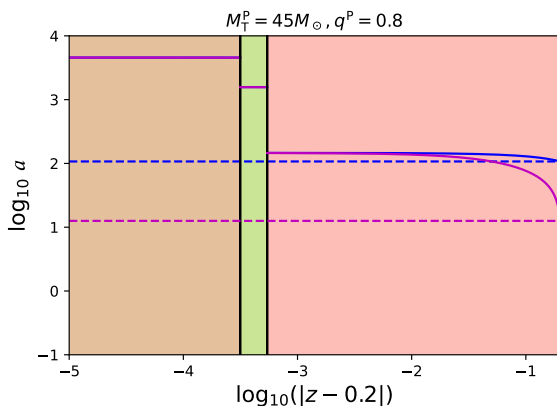


FIG. 1. The figure depicts the evolution of the binary separation parameter a (in units of solar radius R_{\odot}) of a given progenitor as a function of the redshift z . We assume that the progenitors start out at $z = 0.2$ and consists of binary main sequence stars with $M_{\text{T}}^{\text{P}} = 45M_{\odot}$ and $q^{\text{P}} = 0.8$. The left most region of the plot corresponds to $z \sim 0.2$, while the rightmost region is $z \sim 0$. The initial colour shading (brown) corresponds to the star-star phase, the next colour shading (green) corresponds to the star-compact object phase and the final colour shading refers to the situation when both are compact objects. We show our results with ($\rho > 0$) and without ($\rho = 0$) the presence of ULDM. The units of DM density ρ are in GeV/cm^3 . See text for more details.

The results for the evolution of the orbital separation of the binary system, with progenitors having $M_{\text{T}}^{\text{P}} = 45M_{\odot}$ and, $q^{\text{P}} = 0.8$, have been presented in Fig. 1, starting at redshift $z = 0.2$. The evolutionary phases involve the binary components to be either stars or compact objects, e.g., NSs and BHs. Starting from higher redshift values (left hand side of Fig. 1), the different shadings correspond to the binary in its different phases starting from the star-star phase (brown shade), the compact object-star phase (green phase) and finally when both are compact objects (the crimson shade). As per our elaboration of

the baseline model, we notice two discontinuous jumps in the binary separation a across the two endpoints of the main-sequence stars in the binary, following the implementation in Eq. (13). These endpoints of the stars are determined through the mass-luminosity relation of main sequence stars [44], which allows us to compute a simple scaling relation for the lifespan τ_{star} of a star with its progenitor mass M^{P} , namely $\tau_{\text{star}} \propto M^{-2.5}$. Dividing the corresponding quantities for the Sun, and keeping in mind that the estimated life span of Sun is $\tau_{\odot} \approx 10$ Gyr, we obtain the typical lifespan of a star in the binary to be,

$$\tau_{\text{star}}^i (\text{in Gyr}) = \frac{10}{(M_i^{\text{P}})^{2.5}}. \quad (14)$$

Here, i refers to the binary components. We note that owing to the source starting from $z = 0.2$, and the previous relation for the lifespan of main-sequence stars, the binary remains unmerged at $z = 0$ even in the presence of ULDM. However, even the unmerged binaries will carry a signature of the DM environment in their present orbital separation $a_0 \equiv a(z = 0)$, which for the ULDM case is almost half its value for the vacuum configuration (see the horizontal dashed lines in Fig. 1).

We would like to point out that unmerged binaries are effectively binaries in their early inspiral, which cannot be observed by the ground based GW detectors. But, un-merged binaries will show up as nearly monochromatic GWs in the space based detectors, e.g., LISA [45] and DECIGO [46]. Given that the orbital separation a is highly dependent on the density of DM particles in the environment, independent constraints on the ULDM can be obtained from the observation of low-frequency GW signals by LISA [47].

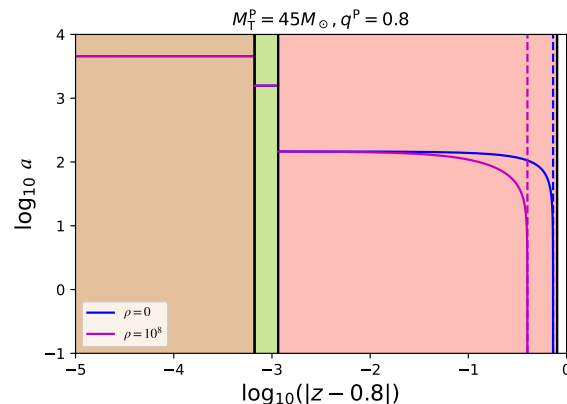


FIG. 2. Same configuration as in Fig. 1, except for the fact that the progenitors start out at $z = 0.8$. In this case, the objects merge at a higher redshift ($z=0.4$) in the presence of ULDM environment, while in vacuum they merge much later, close to $z = 0$. The ‘0’ tick on the x-axis is just to guide the eye.

Finally, we present the effect of ULDM on a similar binary

configuration as before, except for the fact that the binary progenitors now start at a higher value of redshift, namely at $z = 0.8$. This scenario is presented in Fig. 2. In contrast to the previous case, we see that merger happens both in the presence as well as in the absence of ULDM. However, as evident from Fig. 2, the presence of ULDM is seen to make the merger faster, thereby increasing the merger redshift from $z = 0.07$ to $z = 0.4$. This behaviour is expected, and in consonance with the results that we obtained earlier. In short, the dissipation from the ULDM environment adds to the energy loss of the binary, over and above the energy loss from GWs, and consequently we are left with faster merger timescales and/or smaller remnant separation.

B. Evolution of a binary population of progenitors

We have discussed in the previous section how the ULDM environment affects a pair of compact objects undergoing a binary inspiral. In this section we will present the corresponding result for a population of binary progenitors. In doing so, the individual pair of objects can now be thought of as building blocks of a population. To characterise the statistics of merger populations, we need to answer to the question, what happens when many of such individual binaries evolve under a ULDM environment simultaneously. We will answer this question by first considering a toy problem, namely, we will determine the final configuration of a population of binary main-sequence star systems, all of which began at the same redshift. All of these binary systems, during their evolution, undergo accretion from the ULDM environment (if they get converted to BHs) as well as dynamical friction. In addition to these, they will lose energy by emission of GW. The rate of dissipation of the orbital energy, therefore, depends on all the binary parameters (namely masses, spins and eccentricity) as well as on the environment the binary system lives in. Hence, it is clear that the orbital evolution of the binaries will non-trivially depend on the progenitors mass distribution $\{M_i^P\}$ (the so-called initial mass function or, IMF), the spin distribution $\{\chi_i^P\}$ ($\chi \equiv (J/M^2)$, where J is the angular momentum) and the eccentricity distribution $\{e^P\}$ of the population of the progenitor stars and their evolved remnants. The IMF is for the most part unknown, but is expected to be intricately linked to astrophysical factors like stellar metallicity and accretion. The only estimates of the IMF comes from observations of stars in our own galaxy [48] and is usually taken to follow a broken power-law distribution with less massive stars being more probable. Without observation of individual stars, very little can be known about the nature of the IMF [49, 50] in a model independent way at the redshifts of star formation $z \gtrsim 1$. Additionally we also see from the GWTC-3 [51] catalogue that the spin distributions of the remnants cannot still be accurately inferred, while the distributions about eccentricity remain unknown. We

will again opt for the most simplistic formulation possible given the circumstances.

Consequently, we will assume a uniform IMF in order to be maximally agnostic while continuing to assume no effects of eccentricity or BH spin. Moreover, our evolution also does not factor other astrophysical effects like Roche overflows, stellar winds or common envelope binary evolution. We remark that factoring in all of these components that we have left out require a fully numerical population synthesis, which is beyond the scope of this project. The choice of the uniform IMF means that we also need to choose appropriate endpoints in the progenitor stellar-mass distribution. We choose a lower cut-off of the progenitor mass, such that the IMF will have masses satisfying, $M_i^P \geq 10M_\odot$ based on physical considerations. This implies that the stars having masses below this cut-off will not produce compact remnants. Masses of stars are also bounded from above to $M_i^P \leq 100M_\odot$ from considerations of hydrostatic equilibrium. For our purposes in this work, we choose a slightly lower value for the upper limit of the progenitor masses, namely, $M_i^P \leq 80M_\odot$. We argue that the bias produced through this choice will be negligible (compared to other approximations) given that IMF generically exhibits rapid decay for stellar masses above a few solar mass.

We now return to the question of the final state of main sequence star progenitors, all of which evolve in the presence of ULDM, while starting at a fixed redshift. We present the answer to this question in Fig. 3, where we show that the end states of the evolution for progenitor binaries starting from $z = 0.5$. Here and henceforth, we adopt the convention that for the progenitors $M_2^P \leq M_1^P$, such that the mass-ratio $q^P \leq 1$. Following which, in Fig. 3, we show four different panels correspond to four different ambient densities of the ULDM environment. For each panel, we show the mass ratio of the progenitors q^P on the x-axis and the total mass of the binary configuration $M_T^P = M_1^P + M_2^P$ on the y-axis. Following our reasoning above, the grey shaded regions represent configurations that are off-limits to our interest, i.e., with progenitors masses being too high, or, too low. It is expected that the merger timescales for the binary systems will not all be the same, and thus we would get a combination of merged and unmerged binary populations, depending on the DM density in the environment. In Fig. 3, the red line acts as a separatrix, which separates the configuration space into merged and unmerged endpoints for the binaries. The redshifts for the merged population are shown by the green-yellow shade, while for the unmerged populations we depict the binary separation at $z = 0$ by the blue shade.

As evident from Fig. 3, an increase in the ULDM density leads to a reduction in the area under the blue-shaded region, which, as expected, implies more mergers occurring at higher redshifts. Additionally, we observe that a higher ULDM density facilitates

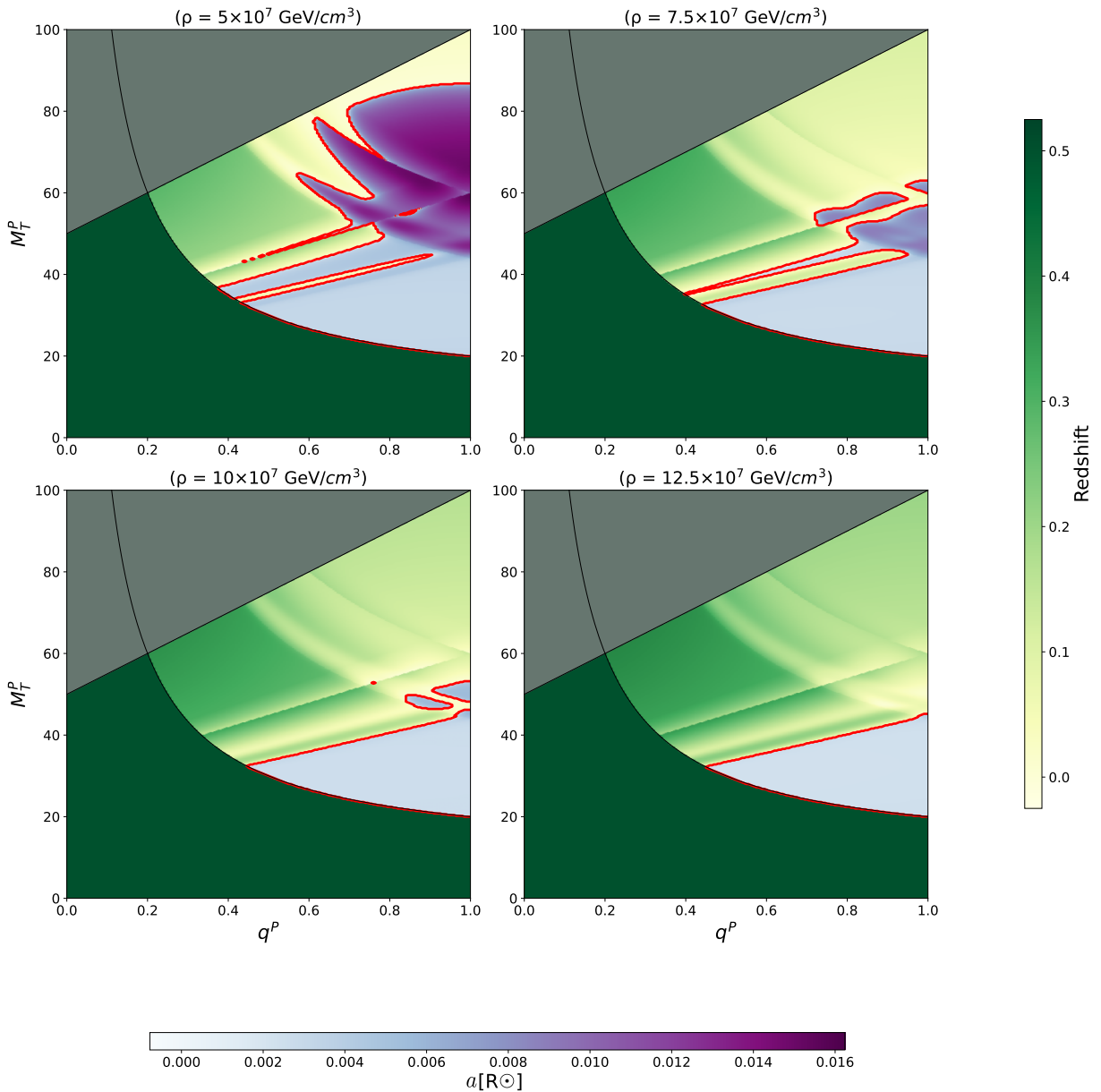


FIG. 3. Plot showing the composition of merged and unmerged final states of all possible combinations of binary main sequence star progenitors beginning at $z = 0.5$. The grey shaded regions are off-limits in progenitor configuration in our modelling (in those regions, either masses are larger than $80M_{\odot}$, or smaller than $10M_{\odot}$). We show the z distribution for the merged cases (green shades) and the binary separation a in units of solar radius R_{\odot} at $z = 0$ for the unmerged cases as a function of the total progenitor masses in the binary and assuming a mass transfer, for different cases of dark matter density. The red line is the separatrix between the unmerged and merged populations at $z = 0$. See text for further details.

the merging of remnants that would otherwise remain unmerged, particularly those originating from more massive progenitors. The oscillatory pattern seen in the parameter space of the unmerged population for $\rho = 5 \times 10^7 \text{ GeV/cm}^3$ (top left plot of Fig. 3) arises from similar oscillatory non-linearities present in our assumed mass-transfer function. Moreover, as the ULDM density increases, its influence becomes more pronounced, eventually overshadowing the mass-transfer effects. This leads to a smoother and more distinct separation between

merged and unmerged regions, as observed for higher values of ρ , e.g., $\rho = 12.5 \times 10^7 \text{ GeV/cm}^3$ (bottom right plot of Fig. 3).

To further quantify these effects, we have presented the fraction of the merged configurations along with the ULDM densities within which they evolve in Table I. Arising out of which we could identify a range of the density of the ULDM environment, namely $1.0 \times 10^7 \text{ GeV/cm}^3 \leq \rho \leq 5.0 \times 10^7 \text{ GeV/cm}^3$, within which

the ULDM remains too rare to induce mergers for binaries starting from $z = 0.5$. However, for densities $\rho \gtrsim 5 \times 10^7 \text{ GeV/cm}^3$, ULDM begins to have a significant impact on the merger fraction, leading to nearly 80% of configurations merging for densities $\sim 10^8 \text{ GeV/cm}^3$ (see Table I). These findings indicate that, within the framework of our simplified toy model, the presence of ULDM influences the evolution of the compact binary populations, systematically increasing the fraction of mergers occurring at earlier cosmic times. While this model is intentionally minimalistic, it serves as an illustrative tool to study how the surrounding dark matter environment can shape merger statistics.

ULDM density in GeV/cm^3	Merger Fraction
0.20×10^7	0.0 %
1.00×10^7	0.0 %
5.00×10^7	43.86 %
7.50×10^7	72.56 %
10.0×10^7	78.89 %
12.5×10^7	80.78 %
15.0×10^7	81.26 %

TABLE I. Table showing the fraction of progenitors that have merged at $z = 0$, starting their orbital evolution at $z = 0.5$, with an increase in the ULDM density ρ . Note that the conservation between the unit for the DM density used in this work with the density in gm/cm^3 is: $1 \text{ GeV/cm}^3 = 1.78 \times 10^{-24} \text{ gm/cm}^3$.

IV. EFFECTS ON ASTROPHYSICAL MERGER RATES

The results of the previous section have firmly established that presence of an ULDM environment should have an effect on the population statistics of mergers. However, we only considered progenitor sources at a single redshift $z = 0.5$. A complete picture can be obtained if we can repeat the above exercise, but factoring in sources from a given range of redshifts. Additionally, we recall that all redshifts will not contribute equally to the generation of compact binary progenitors. This is because the comoving density of main-sequence stars is not constant with the redshift, and has a functional dependence which is well-known in the literature as the Star Formation Rate (SFR). In our analysis in this section, we have used the SFR function, as proposed in Madau & Dickinson [52]. At this outset, we would like to emphasize that the SFR simply provides the total mass of the stars produced at a given redshift per comoving volume. One needs to convolve it with the IMF in order to get the number density of the stars. However in our case this will just be a constant factor, given that our IMF is assumed to be uniform. Subsequent multiplication with the comoving volume results into a function for the number of sources in

the redshift bin z and $z + dz$, which can be observed per unit observer's time. This function, representing number of binary progenitors per unit redshift per unit time, is given by

$$\frac{d^2 N}{dz dt} = \frac{1}{1+z} \left(\frac{dV_c}{dz} \right) \mathcal{R}_\psi(z), \quad (15)$$

where $\mathcal{R}_\psi(z)$ is the SFR at redshift z , and (dV_c/dz) is arising from the cosmological comoving volume. The factor $(1+z)^{-1}$ appears because of the difference in the time intervals at the source and at the observer. Given Eq. (15), we are now in a position to compute the rate of binary compact mergers for our underlying astrophysical model. To compute the ‘merger-rate density’ we need to first evolve all sources at a given z , given by Eq. (15), either to their merger or to $z = 0$. We then bin the population of all the merged events according to their merger redshifts, which gives for us the number $(d^2 N_m/dz_m dt)$, depicting the merger events between redshifts z_m and $z_m + dz_m$, observed per unit observer's time. Here, z_m represents the merger redshifts. Dividing the above by the comoving volume factor at z_m , we finally arrive at our estimate for the merger rate density,

$$\mathcal{R}_m(z_m) \sim \frac{d^2 N_m}{dz_m dt} \left(\frac{dz_m}{dV_c} \right). \quad (16)$$

We can now compare our results and match our estimates of the merger rate $\mathcal{R}_m(z_m)$ to the inferred rate $\mathcal{R}_m^{\text{inf}}(z_m)$ from the LIGO-Virgo observations. But before we do that a word of caution is in order. We reiterate that our baseline model does not contain information about the source IMF and its dependence on z . It also does not consider inputs from many dissipative astrophysical effects (like Roche overflows, common envelope evolutions etc.). Therefore, it is natural to expect overestimation for our calculated merger rates. We should also remark that at current sensitivity, GW observations can only observe the ‘local’ merger rate density $\mathcal{R}_m^{\text{obs}}(0)$, i.e., the merger rate density at $z = 0$. The overestimation can nevertheless be removed by an overall rescaling of the number of sources such that the rescaled estimates of the rate $\mathcal{R}_m(z_m)$ obey observational bounds at $z_m = 0$. In other words, such a rescaling will make $\mathcal{R}_m(0)$ lie within the error bars of $\mathcal{R}_m^{\text{obs}}(0) \equiv R_0$. Subsequently, following this standard procedure in the population synthesis literature (see, for example [53]) we make use of appropriate rescaling functions to bring the value of $\mathcal{R}_m(0)$ within the GWTC-3 bounds [54].

Then in order to make predictions for mergers at higher z_m we have to extrapolate the trends that are observed within the sensitivity horizon of the respective detectors. This is usually done by inferring a power-law behaviour given by a parameter κ for higher z_m from GWTC-3 data. It also should be noted that the bounds on κ come from the observations of BBH systems alone. This is simply because only BBH systems can be observed in enough numbers at $z_m \lesssim 1$ to make inferences about κ

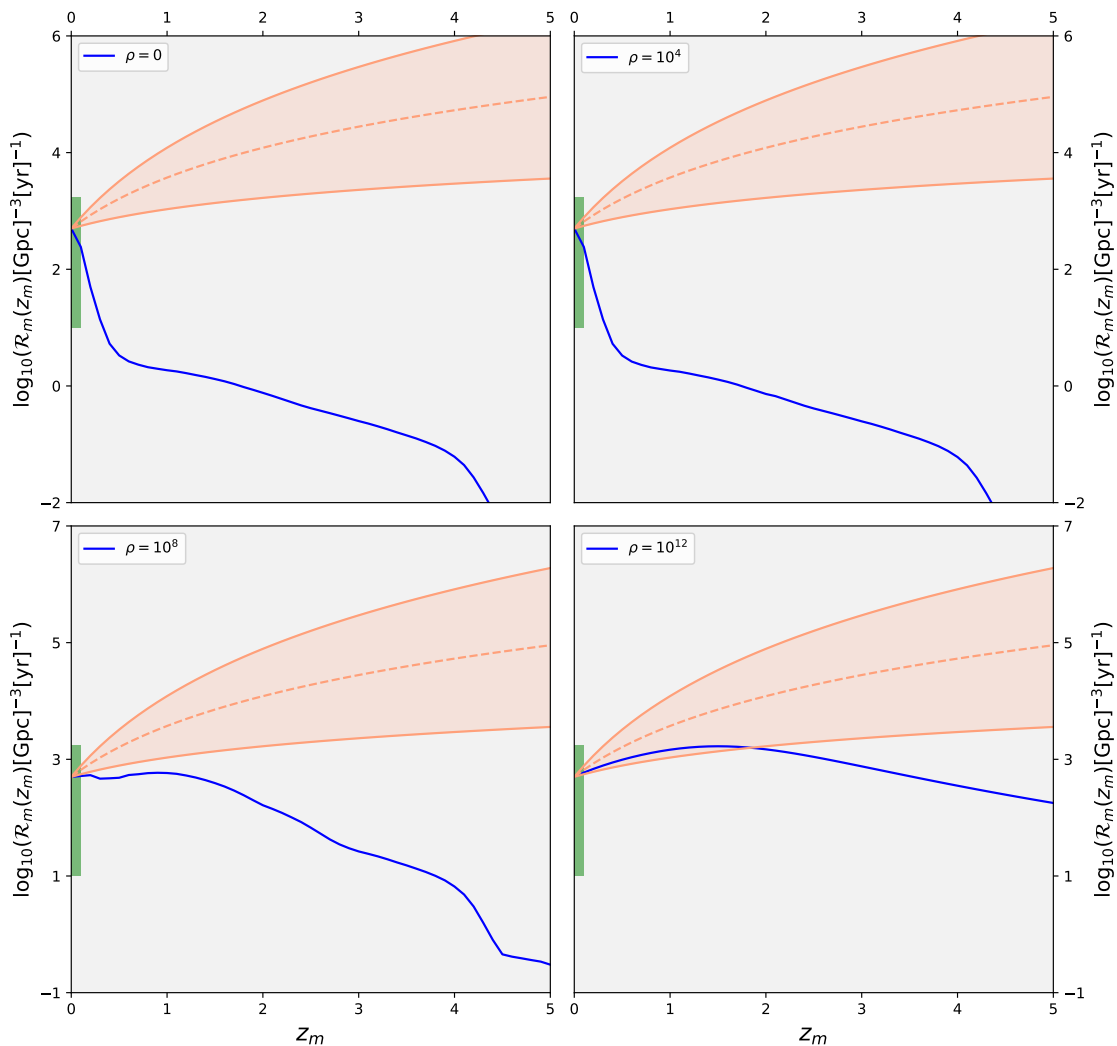


FIG. 4. Plot showing merger rate densities $\mathcal{R}_m(z_m)$ in blue as a function of redshift z for our choices of ULDM density ρ . The green shaded region represents our current uncertainty about the total local merger rate density R_0 of binary compact objects inferred from GWTC-3 data [54]. The red dashed line show the inferred behaviour of the exponent κ of $\mathcal{R}_m^{\text{inf}}(z_m)$ from GWTC-3 data along with its error bars. See text for more details.

using the GWTC-3 detector sensitivity. The overall z_m -dependent statistics of merging compact binaries can then be modelled by a function with two parameters R_0 and κ . We note that the values of these parameters are based on direct observation and extrapolations from inferences respectively. Proceeding this way, we finally arrive at the inferred merger rate $\mathcal{R}_m^{\text{inf}}(z_m)$ given by,

$$\mathcal{R}_m^{\text{inf}}(z_m) \simeq R_0 (1 + z_m)^\kappa . \quad (17)$$

The greatest uncertainty to R_0 (in units of $\text{Gpc}^{-3}\text{yr}^{-1}$) is

contributed by the binary NSs, yielding a very wide range for the merger rate $10 \leq R_0 \leq 1700$ [54]. Consequently we have scaled our populations to have $R_0 = 500 \text{ Gpc}^{-3}\text{yr}^{-1}$, so that our results are consistent with the bounds on R_0 presented by GWTC-3.

Following the previous discussion, we have plotted our rescaled merger rate estimates (blue lines), and the median rate inferred from the GWTC-3 (red dashed lines) for four different choices of the ULDM density in Fig. 4. Then assuming the same allowed value of $R_0 = 500 \text{ Gpc}^{-3}\text{yr}^{-1}$,

we plot the uncertainty region mapped by the 90% credible values of κ as a red shade (see Fig. 4). The uncertainty in R_0 is also depicted as a green shaded region in Fig. 4. Following the convention in [55], the extent of R_0 along the redshift is modelled till $z \sim 0.1$, which is roughly the horizon size of the O3 LVK detectors. We also remark that the reconstruction of $\mathcal{R}_m^{\text{inf}}(z_m)$ from GWTC-3 is mainly based on low redshift ($z_m \lesssim 1$) events, and is therefore not likely to be an accurate representation at $z_m \gtrsim 2$.

The rate estimates plotted in Fig. 4 form our second set of results. We note that in spite of the rescaling applied to $\mathcal{R}_m(z_m)$, its $z_m \lesssim 1$ behaviour for ULDM density $\rho \leq 10^4 \text{GeV/cm}^3$ does not respect the 90% bounds on the power-law exponent as set by GWTC-3. This indicates that the corresponding models can be ruled out at 90% confidence from the GWTC-3 data². Note that we can rule out only the *model*, which is a combination of our baseline model plus ULDM, given by a density of $\rho \leq 10^4 \text{GeV/cm}^3$. We cannot however constrain ULDM ρ in an absolute sense, because the effect of ULDM can be degenerate with the effects of additional dissipative factors like Roche overflow, stellar winds or CE phase evolution. Proceeding in this way, we see that for $\rho = 10^8 \text{GeV/cm}^3$, our model is only marginally consistent with the inferred merger rate for $z_m \sim 0.1$. Finally, ULDM model with DM density, given by $\rho = 10^{12} \text{GeV/cm}^3$ is the best performing. First of all, we see that our merger rate estimation for ULDM density of $\rho = 10^{12} \text{GeV/cm}^3$ agrees with the GWTC power-law bounds for $z_m \lesssim 2$, after which the agreement is lost. This disagreement is actually considerably softened, given that the GWTC power-law bounds themselves are not reliable at such z_m .

The merger rate density also decides the merger probability, which is simply the probability of having a binary merger event between the redshifts of z_m and $z_m + dz_m$, given by the time integral of the quantity ($d^2 N_m / dz_m dt$) defined above. In other words,

$$p_{\text{merg}}(z_m) \sim \int dt \frac{d^2 N_m}{dz_m dt}. \quad (18)$$

We show the merger probabilities of GW events as a function of the merger redshifts z_m , for the present scenario, in Fig. 5. We note that our findings in Fig. 5 are consistent with our previous results. Specifically, we obtained in Section III A that denser ULDM environments tend to reduce merger timescales and make individual binaries merge faster, leading to a greater proportion of merged binaries among progenitors from a given source. In terms of a population with a source distribution, this simply means that with shrinking merger timescales, the peak of the resulting merger distributions should

move towards higher values of z_m . We see that this prediction is exactly reproduced by our results for p_{merg} in Fig. 5. While the ULDM density $\rho = 10^4 \text{GeV/cm}^3$ is indistinguishable from the baseline model without DM, for densities $\rho \geq 10^8 \text{GeV/cm}^3$ the merger probability indeed shifts to the right. The redshift at the peak of the merger probability distribution is thus an observable, which carries the signature of ULDM density ρ . However, with the current GW detector sensitivity, it is not possible to faithfully recreate the merger probability distribution of the GW events. We remark that improvements in ground-based GW detectors would overcome this difficulty and put another independent constraint upon the ULDM environments through direct observation of the peak in the merger redshift for merger probability distribution.

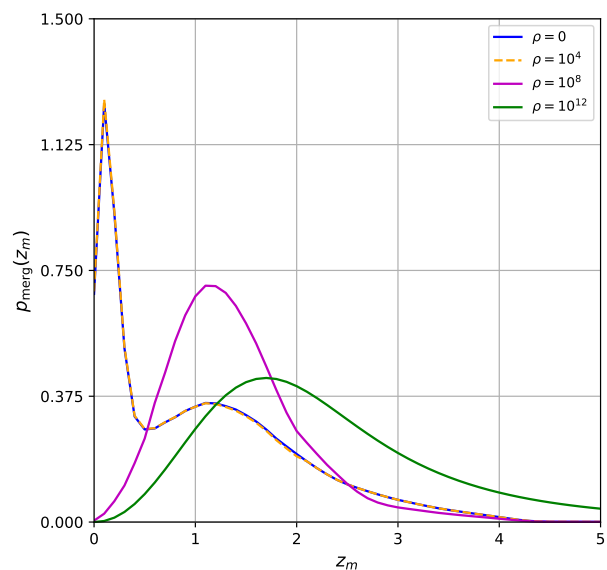


FIG. 5. Plot showing the merger probability distribution as a function of the redshift z for four different choices of the ULDM density ρ . As evident, increasing ρ leads to more merger happening at larger redshifts, leading to a shift of the peak of the merger distribution towards higher redshifts. See text for more details.

V. CONCLUSION

Given that astrophysical environments have previously been found to have non-trivial effects on the GW phasing and merger timescale of individual binaries, it is natural to expect that these environments also leave a significant imprint on their merger statistics. However, baryonic environments are highly case-specific and cannot be assumed to be present for every member of a merger population. In contrast, this situation is notably different for ULDM, as DM is expected to be present in all galaxies, and ULDM are also possibly present in the core region of

² Of course, there are several astrophysical uncertainties in our baseline model, starting from constant IMF, to ignoring Roche overflow.

a galaxy to avoid the core-cusp problem, where compact binary mergers can potentially occur. This ubiquity makes ULDM an intriguing candidate for studying environmental effects on merger statistics. Specifically, additional energy loss through dynamical friction, as the binaries moves in a DM environment, is expected to influence the distribution of the merger timescales, systematically shifting the merger populations toward shorter timescales. It is within this framework that the significance of our work becomes apparent.

In this study, we have performed a series of investigations aimed at quantifying the effects of ULDM and examining whether and how it can influence merger statistics of binaries. Our approach employs a simplified implementation of both the baseline astrophysical model and the DM medium. This is, however, just a toy model, constructed with the primary objective of providing a minimal yet insightful framework to illustrate and analyze the influence of a dark matter environment on merger statistics. The goal is not to present a fully realistic astrophysical model but rather to explore the key qualitative effects that arise when compact binaries evolve within a ULDM background.

Despite these simplifying assumptions, our analysis clearly demonstrates that ULDM fields can indeed impact merger statistics, particularly when their density exceeds the threshold of $\rho > 10^4 \text{GeV/cm}^3$. We started by considering individual binaries and then probing how their merger time gets modified. As expected, and as clearly depicted in Fig. 1 and Fig. 2, the binaries in the DM environment merges quickly compared to the binary that evolves in vacuum. For example, in the case of a binary with total mass $45M_{\odot}$ and mass-ratio of 0.8, the binary with a ULDM environment with DM density $\rho = 10^8 \text{GeV/cm}^3$ merges at $z = 0.4$, while in absence of DM environment merges at $z = 0.07$, while they both start at $z = 0.8$. Thus there is a significant effect on the merger timescale.

This feature continues to hold even for a binary population, where also, the presence of ULDM leads to significantly higher proportion of mergers compared to the vacuum case. In particular, for $\rho > 10^8 \text{GeV/cm}^3$, almost 80% of the original progenitor binary configurations have

merged. This also influences the merger rate of binaries. As evident from Fig. 4, the DM densities below the threshold value of 10^4GeV/cm^3 , the merger rate is in tension with the LVK estimation of the merger rate. This seems to be a tantalizing evidence for the existence of DM, but then the uncertainties in the baseline model, along with various astrophysical considerations can tame this result. Thus, we would like to conclude that merger rate densities can provide a gold mine of information about the existence, and possibly, the nature of DM, provided we have better estimates of the merger rate at higher redshifts and more refined baseline model. Specifically, we have shown that increasing the density of the DM medium leads to a shift in the peak of the merger probability distribution towards higher redshifts. This is expected, as the DM density increases the dynamical friction also increases, leading to an enhanced loss of the orbital energy for the dipole. As a consequence, most of the binaries lose energy faster and hence merges at a higher redshift, i.e., earlier than expected from a vacuum environment. Thus the peak of the merger probability distribution in redshift is another observable that can tell us a lot about the existence and nature of the DM environment in galaxies. These results highlight the potential role of ULDM in shaping the observable characteristics of compact binary mergers and hence provides a novel perspective on how DM may influence astrophysical merger events.

ACKNOWLEDGEMENTS

The authors acknowledge the use of the *Noether* workstation at the Department of Physics, IIT Gandhinagar. The research of KC is supported by the PPLZ grant (Project No. 10005320/0501) of the Czech Academy of Sciences. The research of SS is supported by the Department of Science and Technology, Government of India, under the ANRF CRG Grant (No. CRG/2023/000545). The research of SC is supported by MATRICS (MTR/2023/000049) and Core Research (CRG/2023/000934) Grants from SERB, ANRF, Government of India. SC also thanks the local hospitality at ICTS through the associateship program, where a part of this work was done.

-
- [1] E. Berti *et al.*, “Testing General Relativity with Present and Future Astrophysical Observations,” *Class. Quant. Grav.*, vol. 32, p. 243001, 2015.
 - [2] C. Bambi, “Astrophysical Black Holes: A Review,” *PoS*, vol. MULTIF2019, p. 028, 2020.
 - [3] I. Vidana, “A short walk through the physics of neutron stars,” *Eur. Phys. J. Plus*, vol. 133, no. 10, p. 445, 2018.
 - [4] B. P. Abbott *et al.*, “GW170817: Observation of Gravitational Waves from a Binary Neutron Star Inspiral,” *Phys. Rev. Lett.*, vol. 119, no. 16, p. 161101, 2017.
 - [5] V. Cardoso and P. Pani, “Testing the nature of dark compact objects: a status report,” *Living Rev. Rel.*, vol. 22, no. 1, p. 4, 2019.
 - [6] E. Barausse, V. Cardoso, and P. Pani, “Environmental effects for gravitational-wave astrophysics,” *Journal of Physics: Conference Series*, vol. 610, p. 012044, May 2015.
 - [7] O. Dreyer, B. J. Kelly, B. Krishnan, L. S. Finn, D. Garrison, and R. Lopez-Aleman, “Black hole spectroscopy: Testing general relativity through gravitational wave observations,” *Class. Quant. Grav.*, vol. 21, pp. 787–804, 2004.

- [8] D. Psaltis, “Probes and Tests of Strong-Field Gravity with Observations in the Electromagnetic Spectrum,” *Living Rev. Rel.*, vol. 11, p. 9, 2008.
- [9] E. Berti, K. Yagi, H. Yang, and N. Yunes, “Extreme Gravity Tests with Gravitational Waves from Compact Binary Coalescences: (II) Ringdown,” *Gen. Rel. Grav.*, vol. 50, no. 5, p. 49, 2018.
- [10] V. Cardoso, E. Franzin, and P. Pani, “Is the gravitational-wave ringdown a probe of the event horizon?” *Phys. Rev. Lett.*, vol. 116, no. 17, p. 171101, 2016, [Erratum: *Phys. Rev. Lett.* 117, 089902 (2016)].
- [11] I. R. Stevens, M. J. Rees, and P. Podsiadlowski, “Neutron stars and planet-mass companions,” *Monthly Notices of the Royal Astronomical Society*, vol. 254, no. 1, pp. 19P–22P, 01 1992.
- [12] B. Posselt, R. Neuhaeuser, and F. Haberl, “Searching for substellar companions of young isolated neutron stars,” *Astronomy & Astrophysics*, vol. 496, no. 2, pp. 533–545, March 2009.
- [13] P. Mafa Takisa, L. L. Leeuw, and S. D. Maharaj, “Model of compact star with ordinary and dark matter,” *Astrophys. Space Sci.*, vol. 365, no. 10, p. 164, 2020.
- [14] P. S. Cole, G. Bertone, A. Coogan, D. Gaggero, T. Karydas, B. J. Kavanagh, T. F. M. Spieksma, and G. M. Tomaselli, “Distinguishing environmental effects on binary black hole gravitational waveforms,” *Nature Astron.*, vol. 7, no. 8, pp. 943–950, 2023.
- [15] G. Bertone, “Dark matter, black holes, and gravitational waves,” *Nucl. Phys. B*, vol. 1003, p. 116487, 2024.
- [16] V. Perlick and O. Y. Tsupko, “Calculating black hole shadows: Review of analytical studies,” *Physics Reports*, vol. 947, p. 1–39, Feb. 2022.
- [17] K. Akiyama *et al.*, “First M87 Event Horizon Telescope Results. IV. Imaging the Central Supermassive Black Hole,” *Astrophys. J. Lett.*, vol. 875, no. 1, p. L4, 2019.
- [18] —, “First Sagittarius A* Event Horizon Telescope Results. V. Testing Astrophysical Models of the Galactic Center Black Hole,” *Astrophys. J. Lett.*, vol. 930, no. 2, p. L16, 2022.
- [19] B. P. Abbott *et al.*, “GW150914: First results from the search for binary black hole coalescence with Advanced LIGO,” *Phys. Rev. D*, vol. 93, no. 12, p. 122003, 2016.
- [20] M. Maggiore *et al.*, “Science Case for the Einstein Telescope,” *JCAP*, vol. 03, p. 050, 2020.
- [21] D. Reitze *et al.*, “Cosmic Explorer: The U.S. Contribution to Gravitational-Wave Astronomy beyond LIGO,” *Bull. Am. Astron. Soc.*, vol. 51, no. 7, p. 035, 2019.
- [22] I. S. Sands *et al.*, “Confronting the Diversity Problem: The Limits of Galaxy Rotation Curves as a tool to Understand Dark Matter Profiles,” 4 2024.
- [23] D. Clowe, M. Bradac, A. H. Gonzalez, M. Markevitch, S. W. Randall, C. Jones, and D. Zaritsky, “A direct empirical proof of the existence of dark matter,” *Astrophys. J. Lett.*, vol. 648, pp. L109–L113, 2006.
- [24] K. C. Freeman, “Dark Matter in Dwarf Galaxies,” in *Nearly Normal Galaxies. From the Planck Time to the Present*, S. M. Faber, Ed., Jan. 1987, p. 317.
- [25] R. Massey, T. Kitching, and J. Richard, “The dark matter of gravitational lensing,” *Rept. Prog. Phys.*, vol. 73, p. 086901, 2010.
- [26] M. K. Gaillard, P. D. Grannis, and F. J. Sciulli, “The Standard model of particle physics,” *Rev. Mod. Phys.*, vol. 71, pp. S96–S111, 1999.
- [27] G. R. Blumenthal, S. M. Faber, J. R. Primack, and M. J. Rees, “Formation of Galaxies and Large Scale Structure with Cold Dark Matter,” *Nature*, vol. 311, pp. 517–525, 1984.
- [28] L. Hernquist, N. Katz, D. H. Weinberg, and J. Miralda-Escude, “The Lyman alpha forest in the cold dark matter model,” *Astrophys. J. Lett.*, vol. 457, p. L51, 1996.
- [29] R. Li, C. S. Frenk, S. Cole, L. Gao, S. Bose, and W. A. Hellwing, “Constraints on the identity of the dark matter from strong gravitational lenses,” *Mon. Not. Roy. Astron. Soc.*, vol. 460, no. 1, pp. 363–372, 2016.
- [30] G. Gentile, P. Salucci, U. Klein, D. Vergani, and P. Kalberla, “The Cored distribution of dark matter in spiral galaxies,” *Mon. Not. Roy. Astron. Soc.*, vol. 351, p. 903, 2004.
- [31] J. Kormendy, N. Drory, R. Bender, and M. E. Cornell, “Bulgeless Giant Galaxies Challenge Our Picture of Galaxy Formation by Hierarchical Clustering,” *Astrophys. J.*, vol. 723, no. 1, pp. 54–80, Nov. 2010.
- [32] A. A. Klypin, A. V. Kravtsov, O. Valenzuela, and F. Prada, “Where are the missing Galactic satellites?” *Astrophys. J.*, vol. 522, pp. 82–92, 1999.
- [33] E. G. M. Ferreira, “Ultra-light dark matter,” *Astron. Astrophys. Rev.*, vol. 29, no. 1, p. 7, 2021.
- [34] F. F. Freitas, C. A. R. Herdeiro, A. P. Morais, A. Onofre, R. Pasechnik, E. Radu, N. Sanchis-Gual, and R. Santos, “Ultralight bosons for strong gravity applications from simple Standard Model extensions,” *JCAP*, vol. 12, no. 12, p. 047, 2021.
- [35] R. Vicente and V. Cardoso, “Dynamical friction of black holes in ultralight dark matter,” *Phys. Rev. D*, vol. 105, no. 8, p. 083008, 2022.
- [36] S. Chandrasekhar, “Dynamical Friction. I. General Considerations: the Coefficient of Dynamical Friction,” *Astrophys. J.*, vol. 97, p. 255, Mar. 1943.
- [37] G. Caneva Santoro, S. Roy, R. Vicente, M. Haney, O. J. Piccinni, W. Del Pozzo, and M. Martinez, “First Constraints on Compact Binary Environments from LIGO-Virgo Data,” *Phys. Rev. Lett.*, vol. 132, no. 25, p. 251401, 2024.
- [38] R. Abbott *et al.*, “GWTC-2: Compact Binary Coalescences Observed by LIGO and Virgo During the First Half of the Third Observing Run,” *Phys. Rev. X*, vol. 11, p. 021053, 2021.
- [39] S. Mitra, S. Chakraborty, R. Vicente, and J. C. Feng, “Probing the quantum nature of black holes with ultralight boson environments,” *Phys. Rev. D*, vol. 110, no. 8, p. 084012, 2024.
- [40] S. Roy and R. Vicente, “Compact Binary Coalescences in Dense Environments Can Pose as in Vacuum,” 10 2024.
- [41] C. M. Will and A. G. Wiseman, “Gravitational radiation from compact binary systems: Gravitational wave forms and energy loss to second postNewtonian order,” *Phys. Rev. D*, vol. 54, pp. 4813–4848, 1996.
- [42] C. L. Fryer, K. Belczynski, G. Wiktorowicz, M. Dominik, V. Kalogera, and D. E. Holz, “Compact Remnant Mass Function: Dependence on the Explosion Mechanism and Metallicity,” *Astrophys. J.*, vol. 749, no. 1, p. 91, Apr. 2012.
- [43] K. Chakravarti, R. Ghosh, and S. Sarkar, “Formation and stability of area quantized black holes,” *Phys. Rev. D*, vol. 109, no. 4, p. 046001, 2024.
- [44] M. Salaris and S. Cassisi, *Evolution of Stars and Stellar Populations*, 2005.

- [45] N. Karnesis *et al.*, “The Laser Interferometer Space Antenna mission in Greece White Paper,” *Int. J. Mod. Phys. D*, vol. 33, no. 07n08, p. 2450027, 2024.
- [46] S. Kawamura *et al.*, “Current status of space gravitational wave antenna DECIGO and B-DECIGO,” *PTEP*, vol. 2021, no. 5, p. 05A105, 2021.
- [47] F. Duque, C. F. B. Macedo, R. Vicente, and V. Cardoso, “Extreme-Mass-Ratio Inspirals in Ultralight Dark Matter,” *Phys. Rev. Lett.*, vol. 133, no. 12, p. 121404, 2024.
- [48] P. Kroupa, “On the variation of the initial mass function,” *Mon. Not. Roy. Astron. Soc.*, vol. 322, p. 231, 2001.
- [49] P. Kroupa, C. Weidner, J. Pflamm-Altenburg, I. Thies, J. Dabringhausen, M. Marks, and T. Maschberger, “The Stellar and Sub-Stellar Initial Mass Function of Simple and Composite Populations,” in *Planets, Stars and Stellar Systems. Volume 5: Galactic Structure and Stellar Populations*, T. D. Oswalt and G. Gilmore, Eds., 2013, vol. 5, p. 115.
- [50] T. Jeřábková, A. H. Zonoozi, P. Kroupa, G. Beccari, Z. Yan, A. Vazdekis, and Z. Y. Zhang, “Impact of metallicity and star formation rate on the time-dependent, galaxy-wide stellar initial mass function,” *Astronomy & Astrophysics*, vol. 620, p. A39, Nov. 2018.
- [51] R. Abbott *et al.*, “GWTC-3: Compact Binary Coalescences Observed by LIGO and Virgo during the Second Part of the Third Observing Run,” *Phys. Rev. X*, vol. 13, no. 4, p. 041039, 2023.
- [52] P. Madau and M. Dickinson, “Cosmic Star Formation History,” *Ann. Rev. Astron. Astrophys.*, vol. 52, pp. 415–486, 2014.
- [53] F. Calore, A. Cuoco, T. Regimbau, S. Sachdev, and P. D. Serpico, “Cross-correlating galaxy catalogs and gravitational waves: a tomographic approach,” *Phys. Rev. Res.*, vol. 2, p. 023314, 2020.
- [54] R. Abbott *et al.*, “Population of Merging Compact Binaries Inferred Using Gravitational Waves through GWTC-3,” *Phys. Rev. X*, vol. 13, no. 1, p. 011048, 2023.
- [55] V. Baibhav, E. Berti, D. Gerosa, M. Mapelli, N. Giacobbo, Y. Bouffanais, and U. N. Di Carlo, “Gravitational-wave detection rates for compact binaries formed in isolation: LIGO/Virgo O3 and beyond,” *Phys. Rev. D*, vol. 100, no. 6, p. 064060, 2019.